

Concurrent Fast Growth of Sub-centimeter Single Crystal Graphene with Controlled Nucleation Density in Confined Channel

Ruizhe Wu^{1†}, Jie Pan^{2†}, Xuewu Ou¹, Qicheng Zhang¹, Yao Ding¹,

Ping Sheng² and Zhengtang Luo^{1,*}

¹Department of Chemical and Biomolecular Engineering and the Hong Kong Branch of Chinese National Engineering Research Center for Tissue Restoration & Reconstruction,

²Department of Physics and William Mong Institute of Nano Science and Technology,
The Hong Kong University of Science and Technology,
Clear Water Bay, Kowloon, Hong Kong, China

Email: keztluo@ust.hk

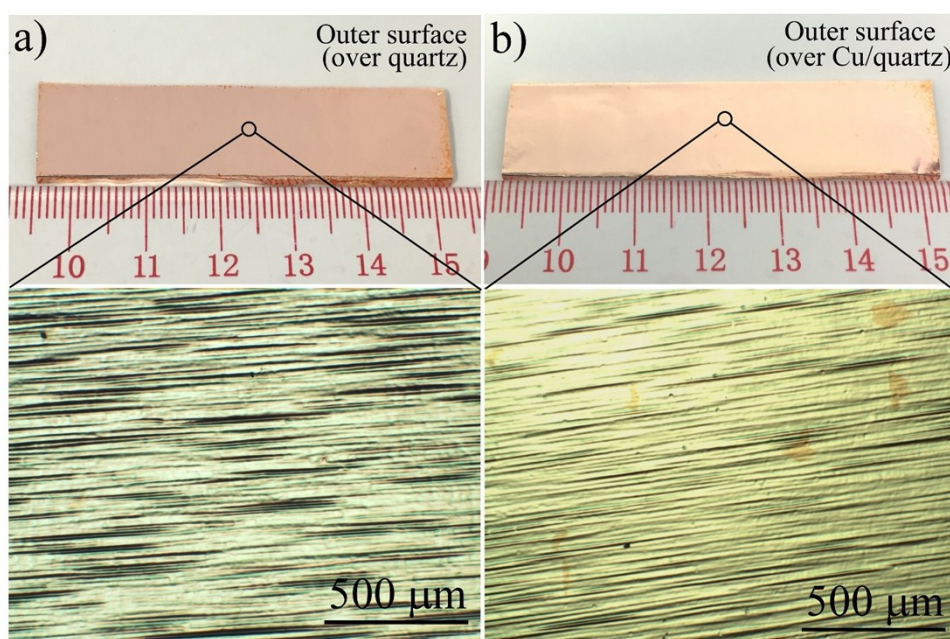


Figure S1. Graphene growth results on the outer surface of Cu foil over (a) quartz substrate and (b) Cu/quartz substrate. In both cases, the outer surface is almost covered by continuous graphene film.

[†] These authors contribute equally to this work.

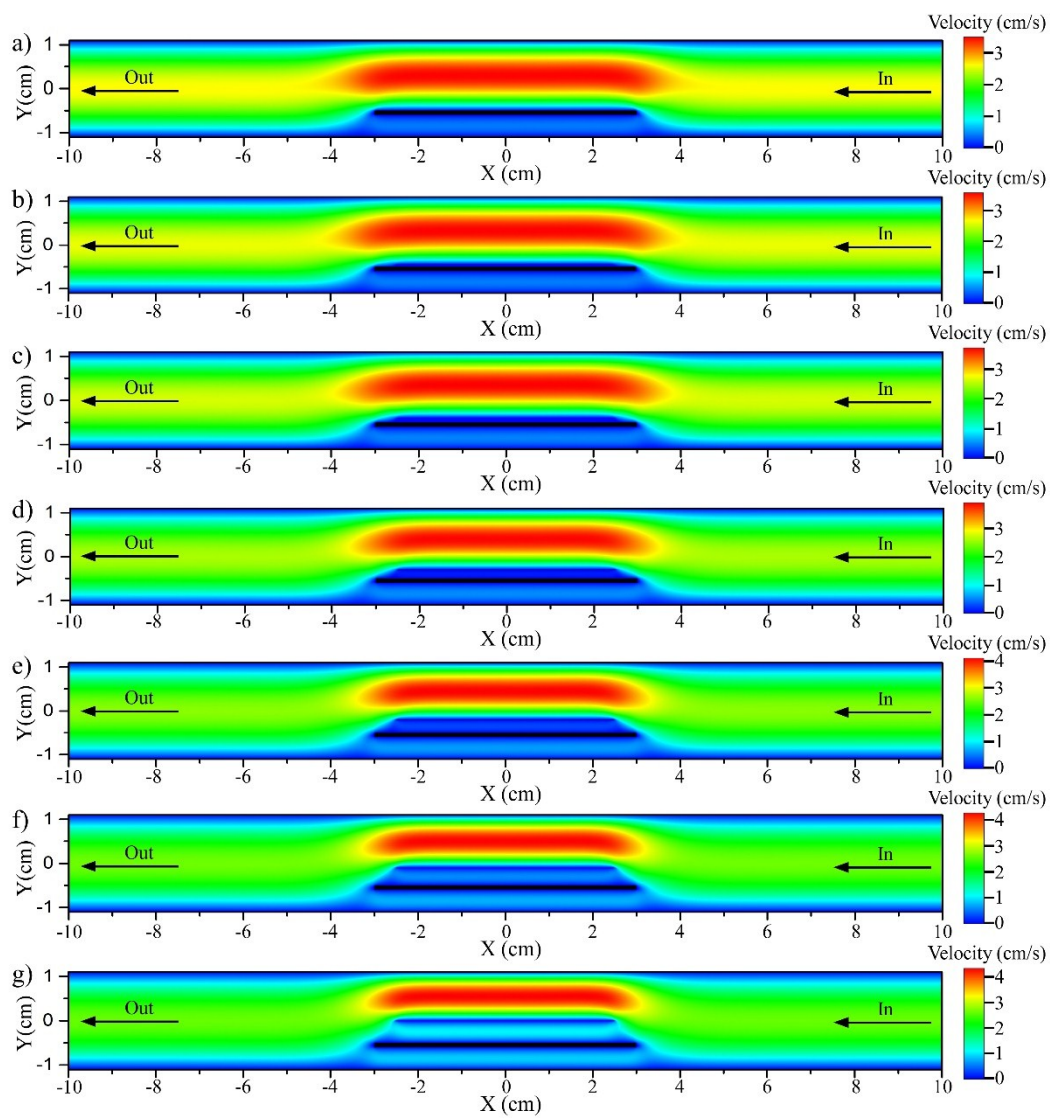


Figure S2. Computation fluid dynamics simulation results of gas velocity distribution in tube with different gap sizes: (a) 0 mm; (b) 0.5 mm; (c) 1 mm; (d) 2 mm; (e) 3 mm; (f) 4 mm; (g) 5 mm.

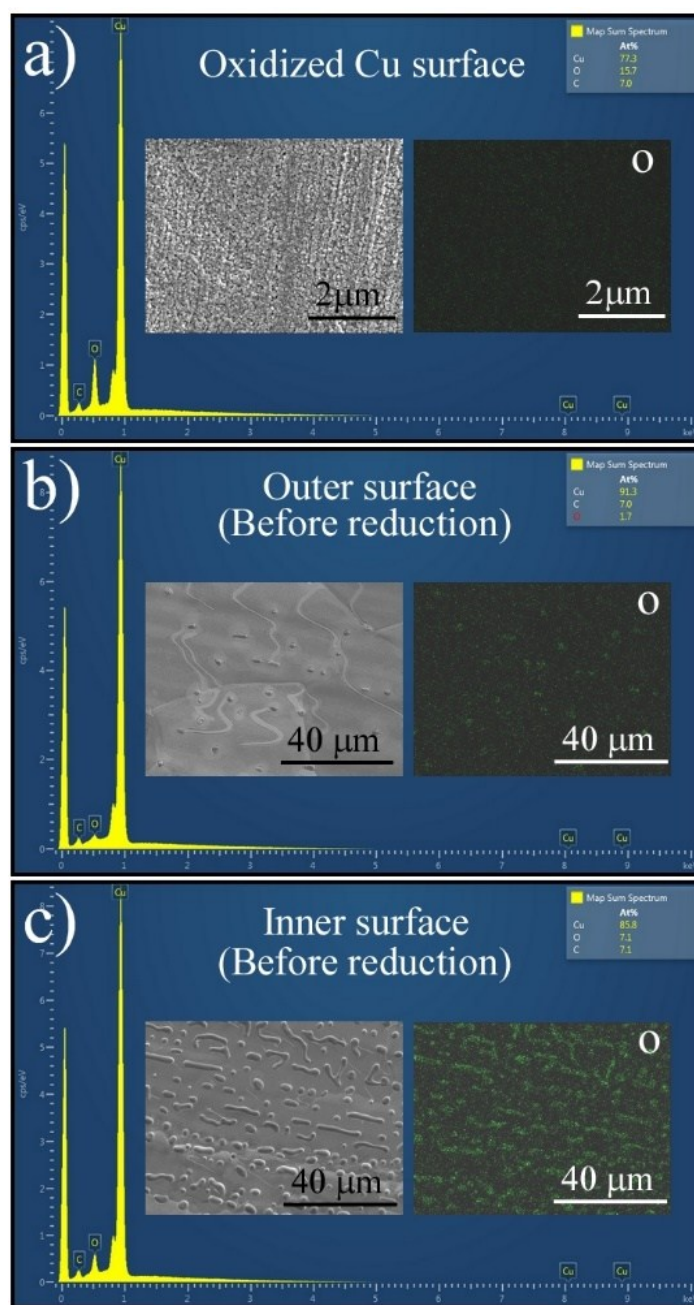


Figure S3. SEM images and EDX results of oxidized copper foil before and after heating to 1050°C in Ar. (a) Before heating in Ar, the surface of oxidized copper foil is covered by oxide nanoparticles with O atomic ratio of 15.7%. (b) After heating in Ar, most oxide particles disappear and the O atomic ratio on the outer surface decreases to 1.7%. (c) After heating in Ar, micrometer sized oxide particles remain and the O atomic ratio on the inner surface decrease to 7.1%.

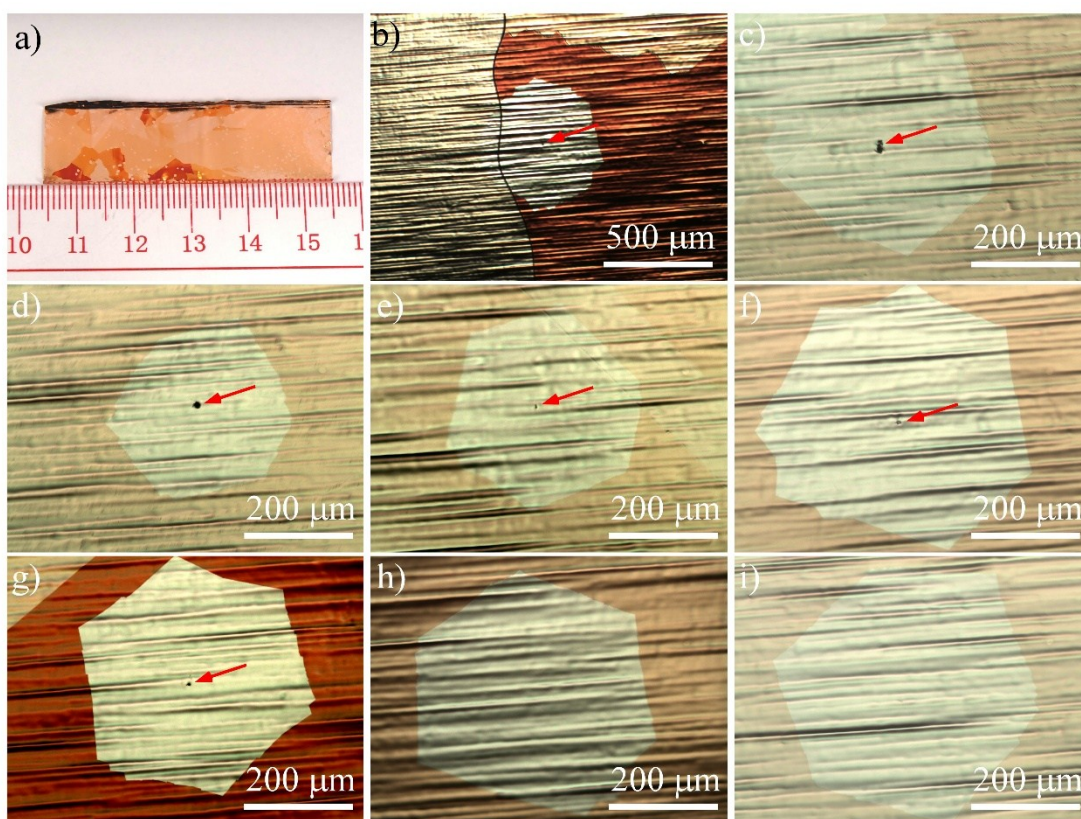


Figure S4. Optical images of graphene grown on the inner surface. (a) Photo of graphene grown on the inner surface. Most graphene grains nucleate at large defective sites which are observable under optical microscope as shown from (b) to (g).

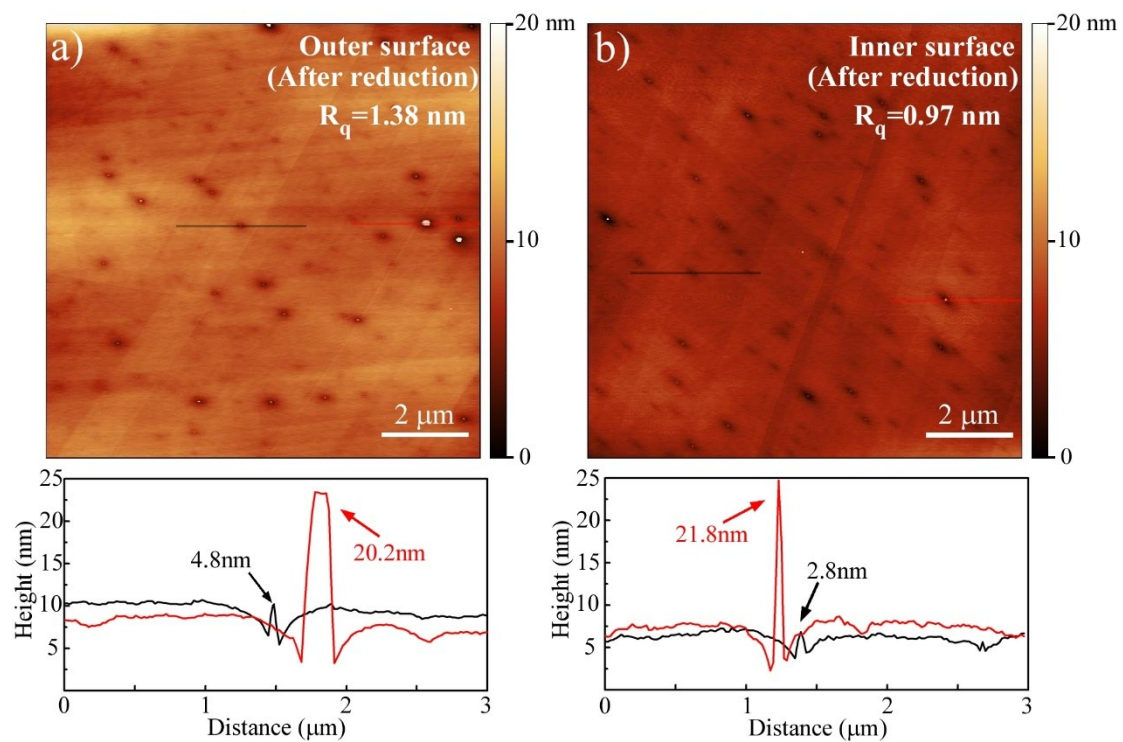


Figure S5. Similar AFM images of outer and inner Cu surface after H_2 reduction. Both surfaces are quite flat with similar roughness value. In addition, there are also some copper nanoparticles on the surface similar to our previous work.

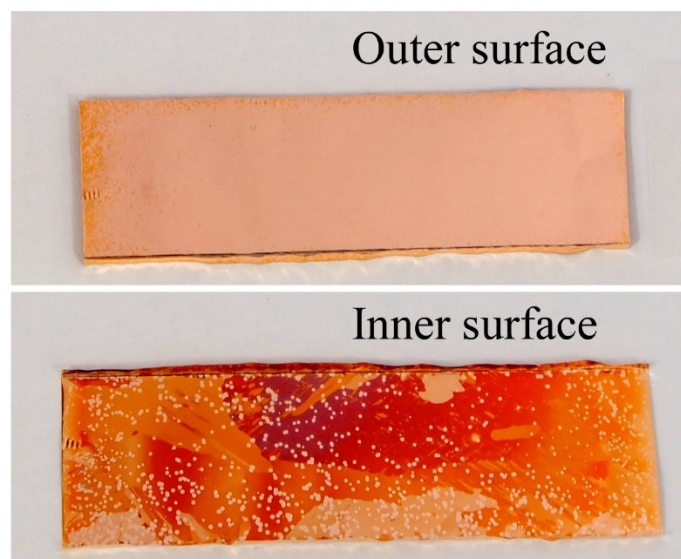


Figure S6. Graphene growth results on both Cu foil surfaces without the pre-oxidation step. The outer surface is almost covered by continuous graphene with a very high nucleation density. The graphene nucleation density is much higher than that in Figure 1 with pre-oxidation step on the inner surface, but still much lower than that on the outer surface. This result indicates that the pre-oxidation step adopted here does not directly result in the nucleation density difference on both Cu foil surfaces.

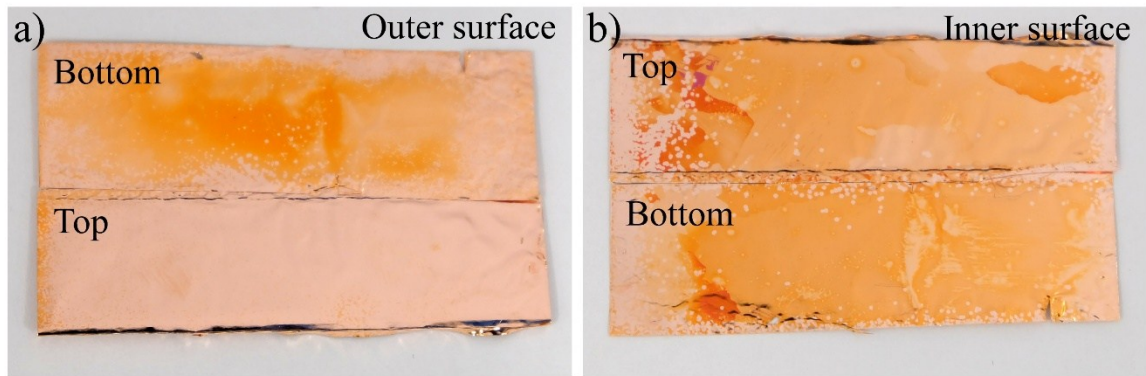


Figure S7. Graphene growth results of both surfaces of Cu foil after inserting a Cu foil between quartz substrate and edge-folded Cu foil. (a) The outer surface of edge-folded Cu foil on top is almost covered with continuous graphene film similar to above results. The graphene grains concentrate at the edges of the inserted Cu foil contacting with quartz substrate on bottom due to limited gas diffusion. (b) The graphene nucleation density on both inner surfaces of the edge-fold and inserted Cu foil is quite low similar to the previous case without inserting another Cu foil. This observation suggests the nucleation density suppression on inner Cu foil surface is not resulted from the released oxygen of quartz substrate.

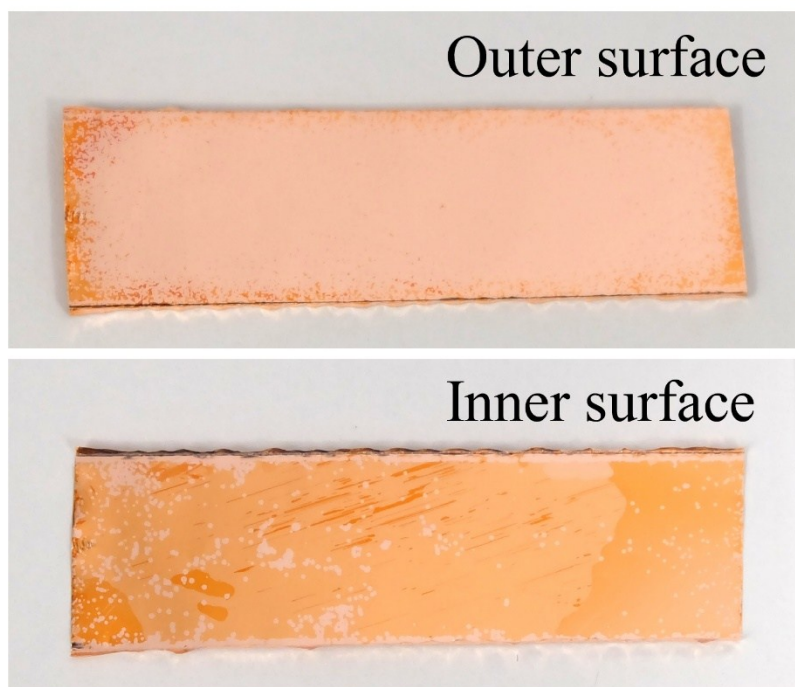


Figure S8. Graphene growth results on both reversed surfaces after hydrogen reduction. The new outer surface (previous inner surface during reduction) is almost covered with continuous graphene film, while the graphene nucleation density is much lower on the new inner surface (previous outer surface during reduction).

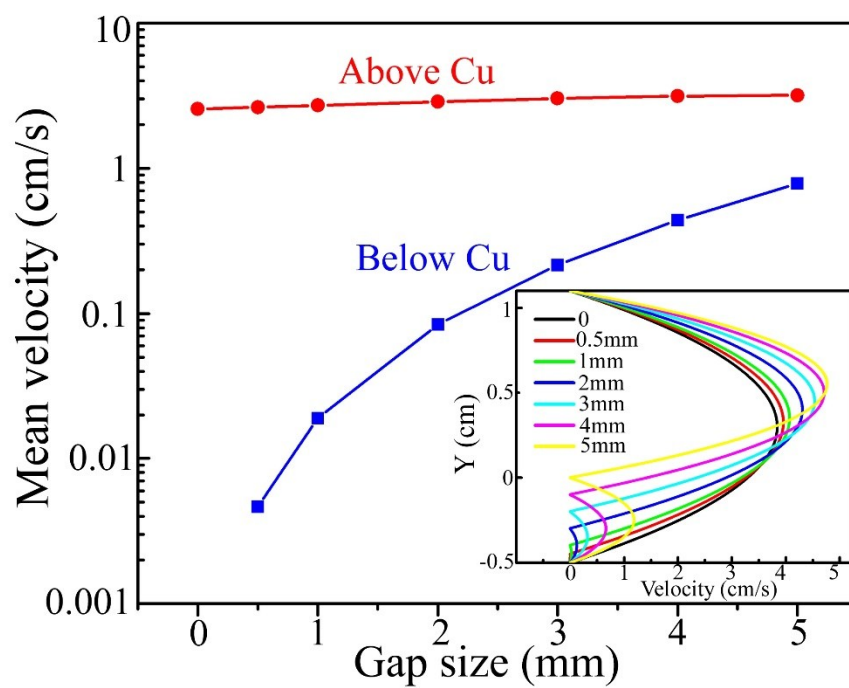


Figure S9. Mean gas flow velocity for different gap sizes extracted from simulation results. The inset shows the detailed central velocity profile.

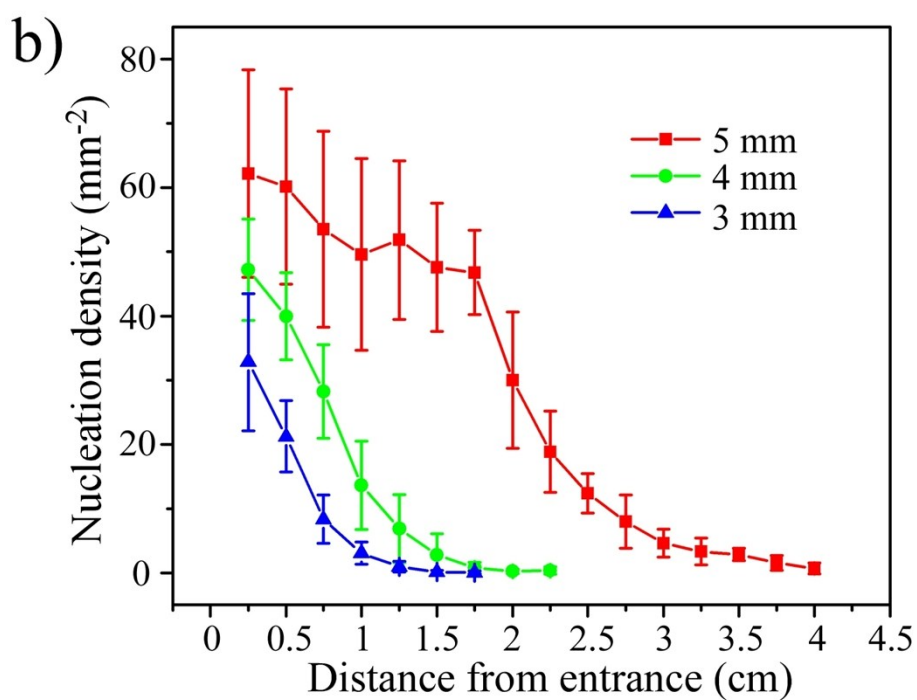
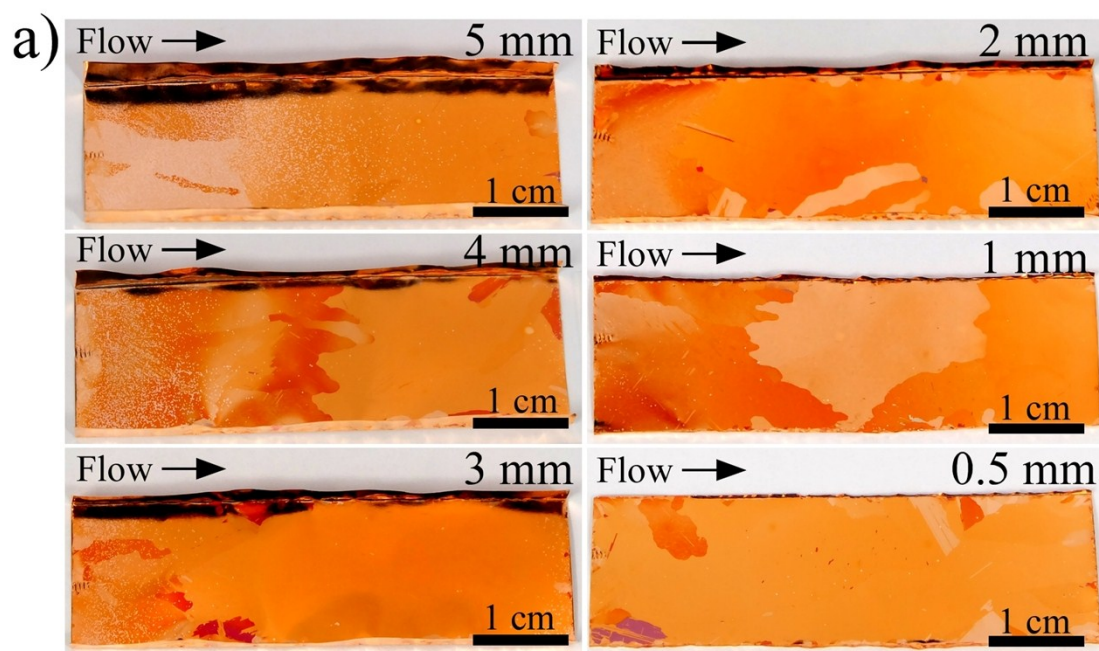


Figure S10. (a) The nucleation density distribution after 5 min growth on the inner surface of the Cu foil with different channel gap sizes. The nucleation density at the gas inlet area increases significantly when the gap size is larger than 2 mm, while the overall nucleation density is very low for gap size smaller than 3 mm. (b) The decrease of nucleation density along the gas flow direction with gap size of 3, 4, 5 mm.

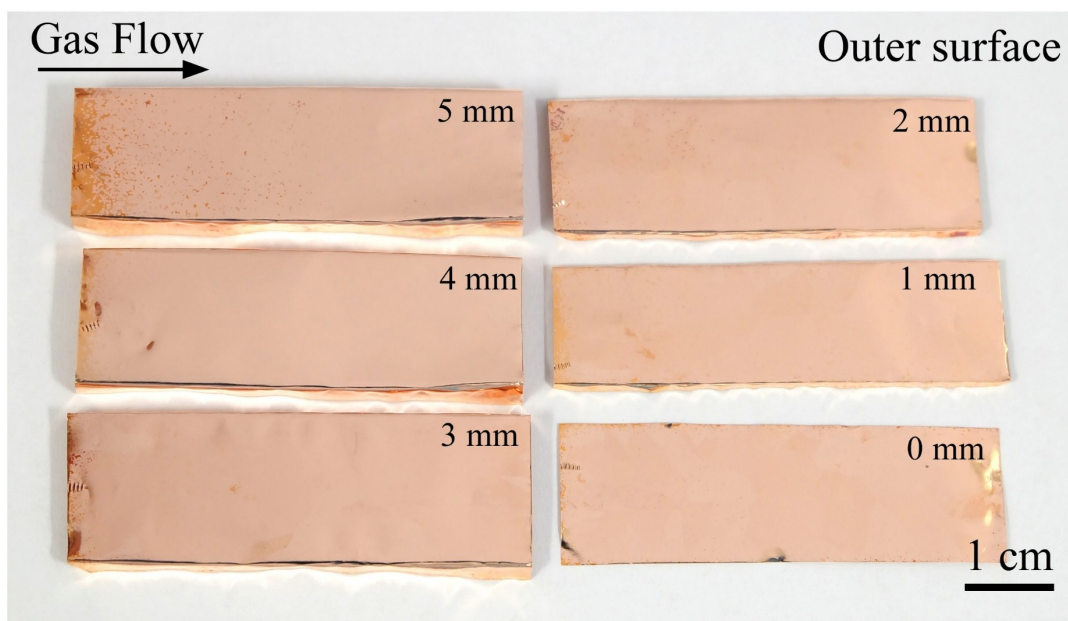


Figure S11. Graphene growth results on the outer surface with different gap sizes (same samples as those in Figure 4a). The nucleation density is very high in all cases as the surface is almost covered by continuous graphene film..

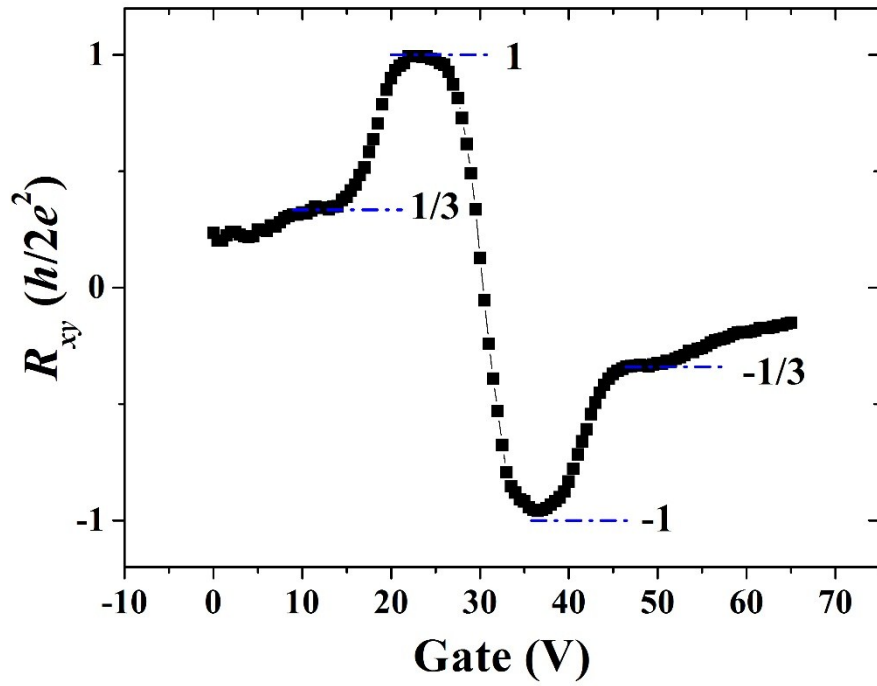


Figure S12. The Quantum Hall effect at $T = 2$ K and $B = 9$ T. The plateau with Hall resistance of ± 1 and $\pm 1/3$ (in the unit of $h/2e^2$) is seen, which is also a clear manifestation of the single-layer nature of our graphene sample.

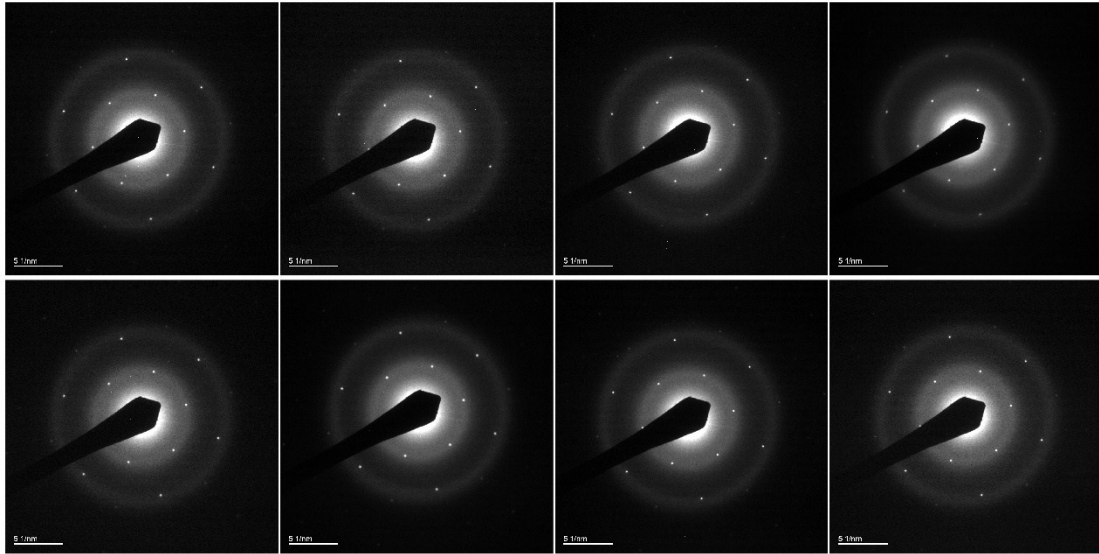


Figure S13. SAED images of millimeter sized fast grown graphene flake transferred onto TEM grid (coated with carbon film) taken from different holes. The same orientation of these images indicates the single crystalline nature of fast grown graphene flake.